

NGTS-19b : A high mass transiting brown dwarf in a 17-day eccentric orbit

Jack S. Acton,^{1*} Michael R. Goad,¹ Matthew R. Burleigh,¹ Sarah L. Casewell,¹ Hannes Breytenbach,^{2,3} Louise D. Nielsen,⁴ Gareth Smith,⁵ David R. Anderson,^{6,7} Matthew P. Battley,^{6,7} Daniel Bayliss,^{6,7} François Bouchy,⁴ Edward M. Bryant,^{6,7} Szilárd Csizmadia,⁸ Philipp Eigmüller,⁸ Samuel Gill,^{6,7} Edward Gillen,^{9,5,†} Nolan Grieves,⁴ Maximilian N. Günther,^{10,‡} Beth A. Henderson,¹ Simon T. Hodgkin,¹¹ James A. G. Jackman,^{12,6,7} James S. Jenkins,^{13,14} Monika Lendl,⁴ James McCormac,^{6,7} Maximiliano Moyano,¹⁵ Richard P. Nelson,⁹ Ramotholo R. Sefako,² Alexis M. S. Smith,⁸ Manu Stalport,⁴ Jessymol K. Thomas,² Rosanna H. Tilbrook,¹ Stéphane Udry,⁴ Richard G. West,^{6,7} Peter J. Wheatley,^{6,7} Hannah L. Worters,² Jose I. Vines,¹³ Douglas R. Alves¹³

¹*School of Physics and Astronomy, University of Leicester, University Road, Leicester, LE1 7RH, UK*

²*South African Astronomical Observatory, P.O Box 9, Observatory 7935, Cape Town, South Africa*

³*Department of Astronomy, University of Cape Town, Rondebosch 7700, Cape Town, South Africa*

⁴*Observatoire de Genève, Université de Genève, 51 Ch. des Maillettes, 1290 Sauverny, Switzerland*

⁵*Astrophysics Group, Cavendish Laboratory, J.J. Thomson Avenue, Cambridge CB3 0HE, UK*

⁶*Centre for Exoplanets and Habitability, University of Warwick, Gibbet Hill Road, Coventry CV4 7AL, UK*

⁷*Dept. of Physics, University of Warwick, Gibbet Hill Road, Coventry CV4 7AL, UK*

⁸*Institute of Planetary Research, German Aerospace Center, Rutherfordstrasse 2., 12489 Berlin, Germany*

⁹*Astronomy Unit, Queen Mary University of London, Mile End Road, London E1 4NS, UK*

¹⁰*Department of Physics, and Kavli Institute for Astrophysics and Space Research, Massachusetts Institute of Technology, Cambridge, MA 02139, USA*

¹¹*Institute of Astronomy, Madingley Road, Cambridge, CB3 0HA, UK*

¹²*School of Earth and Space Exploration, Arizona State University, Tempe, AZ 85287*

¹³*Departamento de Astronomía, Universidad de Chile, Casilla 36-D, Santiago, Chile*

¹⁴*Centro de Astrofísica y Tecnologías Afines (CATA), Casilla 36-D, Santiago, Chile*

¹⁵*Instituto de Astronomía, Universidad Católica del Norte, Angamos 0610, 1270709, Antofagasta, Chile*

Accepted XXX. Received YYY; in original form ZZZ

ABSTRACT

We present the discovery of NGTS-19b a high mass transiting brown dwarf discovered by the Next Generation Transit Survey (NGTS). We investigate the system using follow up photometry from the South African Astronomical Observatory, as well as sector 11 TESS data, in combination with radial velocity measurements from the CORALIE spectrograph to precisely characterise the system. We find that NGTS-19b is a brown dwarf companion to a K-star, with a mass of $69.5^{+5.7}_{-5.4} M_{\text{Jup}}$ and radius of $1.034^{+0.055}_{-0.053} R_{\text{Jup}}$. The system has a reasonably long period of 17.84 days, and a high degree of eccentricity of $0.3767^{+0.0061}_{-0.0061}$. The mass and radius of the brown dwarf imply an age of $0.46^{+0.26}_{-0.15}$ Gyr, however this is inconsistent with the age determined from the host star SED, suggesting that the brown dwarf may be inflated. This is unusual given that its large mass and relatively low levels of irradiation would make it much harder to inflate. NGTS-19b adds to the small, but growing number of brown dwarfs transiting main sequence stars, and is a valuable addition as we begin to populate the so called brown dwarf desert.

Key words: stars:brown dwarfs

* E-mail: ja466@le.ac.uk

† Winton Fellow

1 INTRODUCTION

Brown dwarfs are substellar mass objects which bridge the gap between planets and stars. These are objects with radii similar to that of Jupiter, but with masses ranging between $13 M_{\text{Jup}}$ and $\sim 80 M_{\text{Jup}}$ (Spiegel et al. 2011; Baraffe et al. 2002). The lower mass limit corresponds to the minimum mass at which deuterium burning can occur, below which lie the planets. Whilst the upper mass limit is the classical hydrogen burning limit, above which objects are considered to be low mass stars.

The first unambiguous detections of brown dwarfs were the discoveries of Gilese 229B (Nakajima et al. 1995) and Teide 1 (Rebolo et al. 1995). Since then there have been thousands of brown dwarfs discovered, the vast majority of which are isolated objects discovered by wide field photometric surveys (e.g. Pinfield et al. 2008; Folkes et al. 2012; Reylé 2018; Schneider et al. 2020; Meisner et al. 2020). This is a result of the fact that brown dwarfs cool as they age, due to a lack of nuclear fusion in their cores, making them much easier to detect at the long wavelengths that these surveys typically operate (e.g. WISE; Wright et al. 2010).

Not all brown dwarfs exist in isolated systems. Many have been discovered as companions to main sequence stars, a large number of which have been identified via direct imaging (Nielsen et al. 2019; Vigan et al. 2020). However, brown dwarfs are much fainter than stars, and thus we can only resolve them at large orbital separations. To find close in brown dwarfs, we need to look at the effect they have on their host star (e.g., via transits or radial velocity measurements).

In recent years there have been an increasing number of transiting brown dwarfs discovered around main and pre-main sequence stars by exoplanet surveys (e.g. Csizmadia et al. 2015; Bayliss et al. 2017; Jackman et al. 2019). Given their Jovian sized radii, we would expect these objects to be easy to detect given the vast number of known hot Jupiters around main sequence stars. Similarly, their large masses result in easy to detect radial velocity shifts (km s^{-1} scale rather than m s^{-1} for planetary mass objects) which should also aid in discovery. However despite this, there are just 28 known transiting brown dwarfs around main sequence stars (Carmichael et al. 2020a; Palle et al. 2021), an unusually small number given the fact there are over 4000 known exoplanets¹.

This phenomenon is known as the brown dwarf desert (e.g. Grether & Lineweaver 2006) and was identified as being a dearth of brown dwarfs orbiting main sequence stars within 3 AU, in contrast to the large number of binary stars with close orbits (Marcy & Butler 2000). This was further highlighted by the discovery of large numbers of exoplanets in short period orbits (\sim days), but very few brown dwarfs (Cumming et al. 2008). Recent work with SuperWASP confirmed that this desert still remains (Triaud et al. 2017), despite the vast number of transiting objects discovered by *Kepler* (Borucki et al. 2010) and *TESS* (Ricker et al. 2015). The desert is thought to be a result of the differences between formation mechanisms for planets and brown dwarfs, although recent transiting brown dwarf discoveries have called into question the nature of this so called desert (Carmichael et al. 2019).

Due to their scarcity, it is important that we understand and characterise those transiting brown dwarfs that have been discovered, in particular their masses and radii. Here, transiting brown dwarfs around main sequence stars provide us with an advantage over isolated field brown dwarfs. Their radii can be measured from the depth of their transit in the lightcurve of their host star, whilst

their masses can be measured using radial velocity measurements. Provided the host star parameters are well defined, this allows for accurate determination of these fundamental parameters.

These parameters are particularly valuable when combined with an accurate measurement of system age. As their masses are too small to fuse hydrogen, brown dwarfs cool and undergo gravitational contraction as they age. This contraction occurs most quickly up to an age of 1 Gyr and gradually decreases with time (Baraffe et al. 2003; Saumon & Marley 2008; Burrows et al. 2011; Phillips et al. 2020). With knowledge of the age we can compare the radius of the brown dwarf to that expected by models of gravitational contraction (e.g. Phillips et al. 2020). Equally, we can use a well defined mass and radius measurement to estimate the age of the brown dwarf, by comparing it with stellar isochrones of a variety of ages to see which provides the best fit.

However whilst there are a large number of known brown dwarfs in stellar clusters with well defined ages (Pearson et al. 2020), this is not the case for transiting brown dwarfs. There are very few with accurate age measurements as a result of cluster association (e.g., Gillen et al. 2017; Beatty et al. 2018; David et al. 2019). So the age often needs to be inferred by some other means for example through fitting the spectral energy distribution (SED) of the host star (Choi et al. 2016), or using stellar evolutionary tracks. However this can result in uncertainties of up to a few Gyrs in some cases (e.g. Bayliss et al. 2017; Nowak et al. 2017).

Age measurements are particularly important in the case of transiting brown dwarfs, as we are able to compare the brown dwarf masses and radii to evolutionary models (e.g. Baraffe et al. 2003; Marley et al. 2018). This is one of the best ways to compare the accuracy of these models, as we are comparing them to brown dwarfs whose properties have been directly measured from their interaction with their host stars, allowing for an improved understanding of how these objects evolve as they age. This is particularly important at the high mass ($60\text{--}80 M_{\text{Jup}}$) end of the distribution, where Baraffe et al. (2003) predict the largest changes in radii with age.

It is well established that low mass stars in eclipsing binaries show significant scatter in the relationship between mass, radius and luminosity when compared with evolutionary models (Parsons et al. 2018). However with so few transiting brown dwarfs yet discovered, whether this relationship continues into the substellar regime is unclear. It has been suggested that brown dwarfs may be able to be inflated if they orbit host stars that are particularly active (Casewell et al. 2020). A comparison with evolutionary models would suggest that high mass brown dwarfs are much less likely to be inflated, regardless of the effect of their host star. Additionally, detailed investigation of individual systems has shown that stellar irradiation alone cannot explain discrepancies when they are observed (Beatty et al. 2018). However with so few transiting brown dwarfs known it is challenging to make any clear determination of the cause of these discrepancies. Hence it is important that we discover and characterise as many of these systems as possible.

In this paper we present the discovery of NGTS-19b a high mass brown dwarf in an eccentric 17-day orbit around a main sequence K-star. We make use of high precision photometric and spectroscopic follow up to derive an accurate mass and radius for the brown dwarf. We then place this system in the context of the growing number of brown dwarfs being identified around main sequence stars, and explain how this, and future discoveries will aid in understanding the formation and evolution of these systems.

‡ Juan Carlos Torres Fellow

¹ According to the NASA Exoplanet Archive, March 2021

2 OBSERVATIONS

NGTS-19 was initially discovered using photometry from the Next Generation Transit Survey (hereafter NGTS; (Wheatley et al. 2018)). Follow-up observations were performed with the Sutherland High Speed Optical Cameras (SHOC) (Coppejans et al. 2013) on the South African Astronomical Observatory (SAAO) 1-m telescope. This photometry was then used in conjunction with observations from the Transiting Exoplanet Survey Satellite (TESS, Ricker et al. 2015). We obtained high resolution spectra with the CORALIE Spectrograph (Queloz et al. 2000) to determine the mass of the companion. These observations are detailed in Table 1 and described below.

2.1 NGTS Photometry

Transits of NGTS-19b were initially detected in survey photometry from the Next Generation Transit Survey (Wheatley et al. 2018). NGTS is a wide-field ground based survey for transiting exoplanets operating at ESO’s Paranal observatory in Chile. It consists of an array of 12 fully automated 20 cm telescopes which operate independently to survey large areas of the sky each night. NGTS is optimised for observations of K- and M-type stars, with a custom bandpass range of 520 to 890-nm. NGTS has a wide field of view (instantaneously covering 96 sq deg) and delivers high cadence (every ~ 13 seconds) photometry with high precision (1 mmag per hour for a $I=14$ magnitude star).

NGTS-19 was observed during the 2017 NGTS observing season. The field containing the system (NG1518-2518) was observed for 148 nights between 2017 January 26th and 2017 July 17th, and in total we obtained 200,547 science images at a cadence of 13 seconds. The star is shown in Figure 1. The star is well isolated, and there are no additional Gaia DR2 sources in the NGTS aperture that could dilute the depth of the transit. We also note that none of the nearby Gaia DR2 sources have a parallax or proper motion that is consistent with being physically associated with NGTS-19. The magnitudes of the system in various bandpasses, as well as positional information, is provided in Table 2.

The raw lightcurve was cleaned using an implementation of the SYSREM algorithm (Tamuz et al. 2005). Transits were then detected using the ORION algorithm, which is a custom implementation of the usual Boxed Least Squares (BLS; Kovács et al. 2016) algorithm (see e.g., Wheatley et al. 2018 for more information).

The NGTS observations captured three transits of the system (see Figure 2). From this, ORION detected an orbital period of 17.8 days and transit depth of around 1.5 per cent, corresponding to an object with a radius approximately that of Jupiter. Any shorter period alias could be ruled out by the lack of detection on other nights the star was observed. NGTS candidates are also vetted by a convolutional neural network (CNN) designed to distinguish between transiting signals and false positives (Chaushev et al. 2019). NGTS-19 received a CNN probability of 0.96, strongly suggesting the detection was from a transiting planetary-sized object. This information gave us good confidence that the signal was real, and we decided to undertake follow-up observations.

2.2 TESS Photometry

NGTS-19 was observed by TESS in Sector 11 of the primary mission (TIC-48481940, $T=13.2$ mag). The system was observed between 2019 April 22nd and 2019 May 20th, in the full frame images

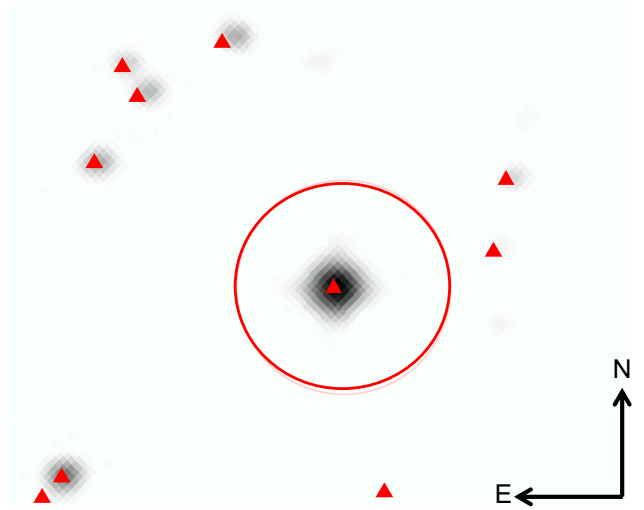


Figure 1. Digital Sky Survey (DSS) image of NGTS-19. The red triangles indicate the positions of nearby objects that are identified in Gaia DR2. The red circle shows the NGTS aperture used to create the NGTS lightcurve. NGTS-19 is the only known source within the aperture used for reduction.

at 30 minute cadence. TESS observed NGTS-19 with CCD 3 of camera 1.

To extract the lightcurve of NGTS-19 from the full-frame images we used a bespoke process, described in more detail in Gill et al. (2020). In short, we use a custom aperture that is selected based on a flux threshold. Background pixels were selected using an iterative sigma clipping process, and pixels where the median counts exceeded 100 times the standard deviation in the background were identified as the source. We then used a floating median to identify and mask out systematic flux drops due to spacecraft effects.

TESS detects two transits of NGTS-19 spaced approximately 17-days apart (see Figure 2). It is worth noting that the TESS observations alone cannot rule out the orbital period of the system being half of this, as a third transit would fall in the data gap in the middle of the sector during spacecraft downlink. However, this potential shorter period is not compatible with either the NGTS photometry (Section 2.1) nor the radial velocity measurements (Section 2.4), which are both compatible with a 17.8 day period, thus highlighting the need for additional data to interpret the TESS photometry. We note that NGTS-19 will be re-observed in TESS sector 38 of the extended mission. Based on our established ephemeris TESS should then observe a further two transits.

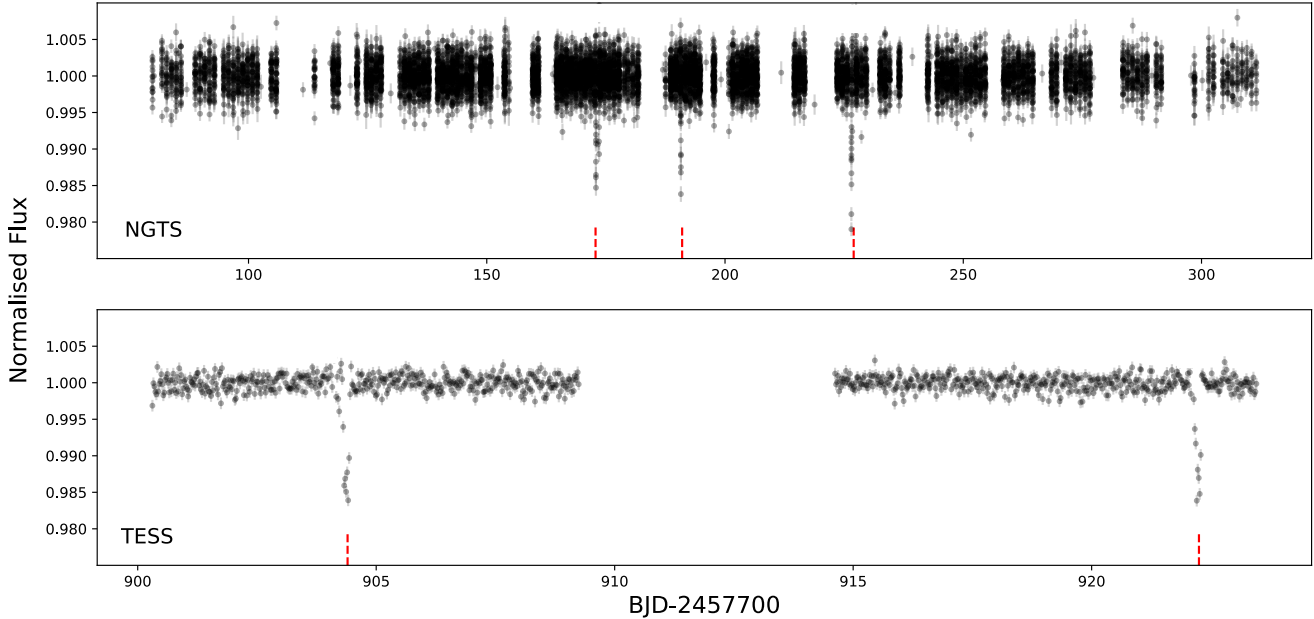
2.3 SAAO Photometry

Due to the period of this system, the combined photometry of NGTS and TESS contained only a small number of transits. Thus we obtained additional photometry of NGTS-19 using the 1-m telescope at SAAO with the SHOC instrument on 2020 July 19th. This would allow us to obtain more precise measurements of the transit depth and width, and thus increase our precision on the radius of the companion. We observed the transit in the V band in order to check for any colour dependent depth difference which may be indicative of a stellar companion. The observation consisted for 400×60 -sec exposures for a total observation time of 6 hours 40 minutes.

The data were bias and flat field corrected via the standard

Table 1. Summary of photometric and spectroscopic observations of NGTS-19.

Observation type	Telescope	Band	Cadence	Total integration time	Period	Notes
Photometry	NGTS	520-890 nm	13 s	148 nights	26/01/17-17/09/17	3 Transits
Photometry	SAAO	V	60 s	400 mins	19/07/20	Single Observation
Photometry	TESS	600-1000 nm	1800 s	28 days	22/04/19-20/05/19	2 Transits
Spectroscopy	CORALIE	390-680 nm	45 mins	4.5 hours	05/02/20-27/02/21	Eight RVs

**Figure 2.** Upper: NGTS Lightcurve of NGTS-19 comprising of 148 nights of observations, binned to 5 minutes. NGTS detects three transits of the system, indicated by the red lines. Lower: TESS Lightcurve for NGTS-19 obtained during sector 11 of the mission (TIC-48419840), observed at 30 minute cadence in full frame images. Two transits are seen during the sector, spaced approximately 17.8 days apart, and are indicated by the red dashed line.**Table 2.** Stellar properties and colour magnitudes for NGTS-19 from 2MASS (Skrutskie et al. 2006), Gaia (Gaia Collaboration et al. 2018), TicV8 (Stassun et al. 2019) and NGTS (Wheatley et al. 2018).

Property	Value	Source
Gaia I.D.	DR2 6226795997504049664	Gaia
TIC I.D.	48481940	TIC v8
R.A. (J2000)	15:16:31.6	NGTS
Dec (J2000)	-25:42:17.24	NGTS
μ_α (mas yr ⁻¹)	-45.796 ± 0.054	Gaia
μ_δ (mas yr ⁻¹)	-14.746 ± 0.038	Gaia
Parallax (mas)	2.6666 ± 0.0285	Gaia
<i>G</i>	13.83	Gaia
NGTS	13.20	NGTS
TESS	13.20	TIC v8
<i>B</i>	15.18	TIC v8
<i>V</i>	14.12	2MASS
<i>J</i>	12.27	2MASS
<i>H</i>	11.82	2MASS
<i>K</i>	11.70	2MASS

procedure, using the SAFPHOT Python package². SAFPHOT was

² <https://github.com/apchsh/SAFPHOT>

also used to carry out differential photometry, by extracting aperture photometry from the target as well as comparison stars using the 'SEP' package (Barbary 2016). SEP also measured and subtracted the sky background, adopting a box size and filter width which minimised the background residuals measured across the frame after the stars had been masked out. Two comparison stars were used to perform differential photometry on the target, with a 3.8 pixel radius aperture selected to maximise the signal-to-noise.

The observation clearly detects the transit, which occurred almost exactly as predicted by the ephemeris from the NGTS and TESS observations. We also note no significant difference in depth between this lightcurve and the NGTS and TESS observations, despite the fact the SAAO data were obtained using a much bluer filter. This adds further confidence to the companion being sub-stellar in nature.

2.4 CORALIE Radial Velocities

To determine the mass and orbital eccentricity of NGTS-19b we obtained spectroscopic observations using the CORALIE spectrograph mounted on the Swiss 1.2-metre Leonhard Euler Telescope at ESO's La Silla Observatory, Chile. CORALIE is an echelle spectrograph fed by a 2 arcsec science fibre, capable of 3 m s⁻¹ RV precision

Table 3. Radial Velocities for NGTS-19 obtained with the CORALIE spectrograph

BJD _{TDB} (-2,450,000)	RV (km/s)	RV error (km/s)	FWHM (km/s)	Contrast (%)	Bisector Span
8884.876	-30.53	0.17	9.68	53.50	-0.097
8885.832	-26.50	0.13	9.57	53.28	-0.239
8903.859	-26.15	0.14	9.43	54.37	0.057
8911.851	-36.73	0.11	9.82	49.47	-0.299
8925.753	-32.27	0.11	9.15	52.78	0.0212
8928.730	-36.14	0.15	9.01	54.19	-0.014
9261.805	-25.77	0.14	9.25	58.78	-0.17
9272.782	-38.40	0.16	9.14	52.94	-0.28

Table 4. NGTS-19 stellar parameters derived using `SPECMATCH-EMP` and `ARIADNE`. The `ARIADNE` parameters are used for the global modelling of the system in Section 3.3.

Parameter	<code>SPECMATCH-EMP</code>	<code>ARIADNE</code>
Teff (K)	4500 ± 110	4716 ⁺³⁹ ₋₂₈
Log g (cm s ⁻²)	4.62 ± 0.12	4.571 ^{+0.102} _{-0.093}
Radius (R _⊙)	0.71 ± 0.10	0.896 ^{+0.040} _{-0.035}
[Fe/H]	0.09 ± 0.09	0.11 ^{+0.074} _{-0.070}
Mass (M _⊙)	0.73 ± 0.08	0.807 ^{+0.038} _{-0.043}
Age (Gyr)	—	8.5 ^{+3.2} _{-6.0}
Distance (pc)	—	371 ⁺¹⁵ ₋₁₂

on bright stars (see e.g. [Rickman et al. \(2019\)](#) for recent results). As NGTS-19 is relatively faint for a telescope of this size ($V = 14.12$), we used long (45 minute) exposures to maximise the signal-to-noise. This allowed for precision on a scale of around 100 m s⁻¹, which is sufficient to distinguish between stellar and sub-stellar companions.

We obtained a total of eight spectra of NGTS-19. These were cross correlated with a binary G2 mask using the standard CORALIE pipeline, while discarding the first 20 spectral orders where the signal-to-noise ratio was less than one. The radial velocity associated with NGTS-19 was extracted from the Cross Correlation Function (CCF) by fitting a Gaussian function. The radial velocity measurements show a large amplitude variation (~ 6.5 km s⁻¹) in phase with the period defined by the NGTS photometry, with a significant level of eccentricity. This suggests the presence of a high mass substellar companion. The full radial velocity measurements are shown in Table 3. We note that one of the points was obtained close to phase 0, however we ensured that this measurement was not taken during the transit of the brown dwarf.

3 ANALYSIS

3.1 Spectral Analysis

We used the CORALIE spectra of NGTS-19 to obtain initial parameters for the system. The CORALIE spectra were shifted in wavelength and co-added to create a single high signal-to-noise spectrum for spectral analysis. However, owing to the faintness of the system this combined spectrum still had a relatively low signal-to-noise ratio (8.28). Nonetheless it was sufficient to obtain some initial system parameters that would be refined in the subsequent analysis.

We analysed this stacked spectrum using the template matching code `SPECMATCH-EMP` ([Yee et al. 2017](#)), which characterises spectra of stars by comparing them with a library of high resolution spectra obtained with Keck/HIRES. `SPECMATCH-EMP` first shifts the input spectrum to the same wavelength scale as the templates, and then compares it to each star in the library to find the best matching individual spectra. Linear combinations of the best matches are then used to create the best match to the input spectrum. Various stellar parameters for the star are then computed based on a weighted average of library parameters from the reference spectra. These properties are shown in Table 4. The parameters calculated by `SPECMATCH-EMP` show that the star is a late K-dwarf with a mass of 0.73 M_⊙. Rather than adopting these as the final parameters for the primary star, we use them as priors for the spectral energy distribution (SED) fitting procedure detailed in 3.2.

It is interesting to note, that from this analysis we constrain the metallicity to a value of +0.1 dex, implying that NGTS-19 is a metal-rich star. Even though in [Jenkins et al. \(2015\)](#) they show that the median brown dwarf host star metallicity is sub-solar, the distribution spans a wide range of values with a flat functional form, unlike the case of giant planets. Here, NGTS-19 adds another example to the metal rich population of brown dwarf host stars, and this time with a measured radius.

Additionally, we used this stacked spectrum to determine the projected stellar rotation velocity ($v \sin(i)$). To do this, we fit synthesised spectra to the spectrum of NGTS-19 using `iSpec` ([Blanco-Cuaresma et al. 2014](#)). We fit only for $v \sin(i)$, fixing the other values to those obtained from `SPECMATCH-EMP`. From this we obtain a value for $v \sin(i)$ of 2.1 ± 0.4 km s⁻¹.

3.2 SED Fitting

To obtain precise parameters for the host star, we performed a fit to the Spectral Energy Distribution. This was done using `ARIADNE` ([Vines & Jenkins 2021](#)), which we describe in brief here. `ARIADNE` is a publicly available Python tool which fits catalogue photometry of stars from various sources (e.g., Gaia, TESS) to various atmospheric model grids. The specific grids used by `ARIADNE` are `Phoenix v2` ([Husser et al. 2013](#)), `BT-Sett1`, `BT-Cond`, `BT-NextGen` ([Allard et al. 2012](#); [Hauschildt et al. 1999](#)), as well as the grids of [Castelli & Kurucz \(2004\)](#), and [Kurucz \(1993\)](#).

We create model SEDs by interpolating these grids in $T_{\text{eff}} - \log g - [\text{Fe}/\text{H}]$ space, with distance, radius and extinction in the V band used as model parameters. An excess noise term was applied for each set of parameters to account for an underestimation of the uncertainties. These were normally distributed around zero with a variance of five times the size of the reported uncertainty. Priors for T_{eff} , $\log g$ and $[\text{Fe}/\text{H}]$ and radius were applied based on the results from `SPECMATCH-EMP` (see Section 3.1). Extinction was limited to the maximum line of sight value taken from the SFD galactic dust map ([Schlegel et al. 1998](#); [Schlafly & Finkbeiner 2011](#)).

The parameters from the SED were estimated using nested sampling performed using the python package `DYNESTY`. This was also used to calculate the Bayesian evidence for each of the individual models. For the fitted parameters, a weighted average is then computed using the relative probabilities of each of the fitted models. This Bayesian model averaging results in a remarkable degree of precision in these parameters when compared with using any one individual model SED fit. Finally, a mass estimate is calculated using a MIST isochrone ([Choi et al. 2016](#)). The results of this fitting are given in Table 4, and the fit to the SED is shown in Figure 3. Based on our SED fit and the classification established by [Pecaut &](#)

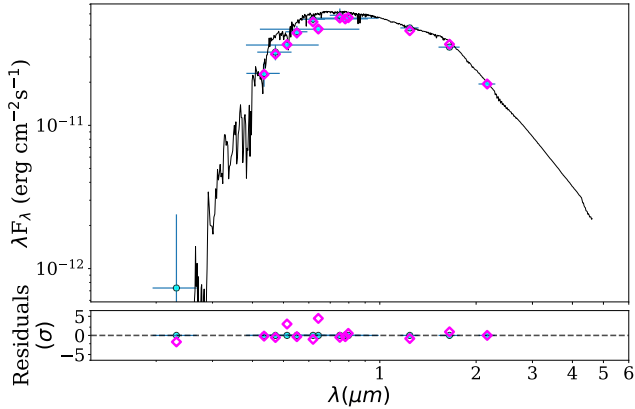


Figure 3. Upper Panel – Spectral energy distribution of NGTS-19. Blue points show the catalogue photometry for the system from a variety of sources, and the magenta diamonds are the synthetic photometry fit. The black line shows the best fitting model. Lower Panel – Residuals to the SED fit, normalised to the photometry errors.

Mamajek (2013), this makes the primary star a K3.5V dwarf. We adopt these parameters for the host star in our subsequent global fitting for this system

3.3 Global Modelling

To determine orbital parameters for the system we jointly modelled the photometry and radial velocities using ALLESFITTER (Günther & Daylan 2019, 2020). ALLESFITTER is a publicly available Python code for performing global modelling of photometric and radial velocity data. The software acts as a wrapper for a number of well-used packages, in particular, we utilise the eclipsing binary light curve modeller ELLC (Maxted 2016) and the Markov Chain Monte Carlo (MCMC) sampler EMCEE (Foreman-Mackey et al. 2013) to simultaneously model the NGTS, TESS, SAAO and CORALIE data. Prior to running the MCMC we perform some simple preparation of the data. The raw lightcurves were normalised to a baseline of 1 by using the median out of transit flux. We then binned the NGTS data to 10 minutes, to reduce computational time. The TESS and SAAO data remained unbinned.

We chose to start the walkers in a region of parameter space that gave a reasonable initial fit to the data. We note that whilst starting the walkers in a random position does not preclude the ability to obtain a good fit to the data, it does increase the burn in time required to do so. Each walker was given a starting position normally distributed around the values we found to give an initial fit. We used values from ORION for the ephemeris of the system, and obtained values for the stellar radius ratio, scaled primary star radius and inclination from an initial fit to the NGTS data alone performed by ORION. Equally, starting positions for the radial velocity parameters were determined by fitting these data alone. We also incorporated a radial velocity jitter term added in quadrature to account for any effects of stellar variability in the RVs, as well as normalisation offsets and systematic errors for the lightcurves. We knew from the radial velocity measurements that there was a significant level of eccentricity in the system, but for the fitting we started the walkers at zero eccentricity and allowed the sampler to determine it. We note that for fitting purposes, ALLESFITTER parameterises eccentricity e , relative to the argument of periastron, ω , using terms $\sqrt{e}\cos(\omega)$ and $\sqrt{e}\sin(\omega)$. Finally, we also determined limb darkening param-

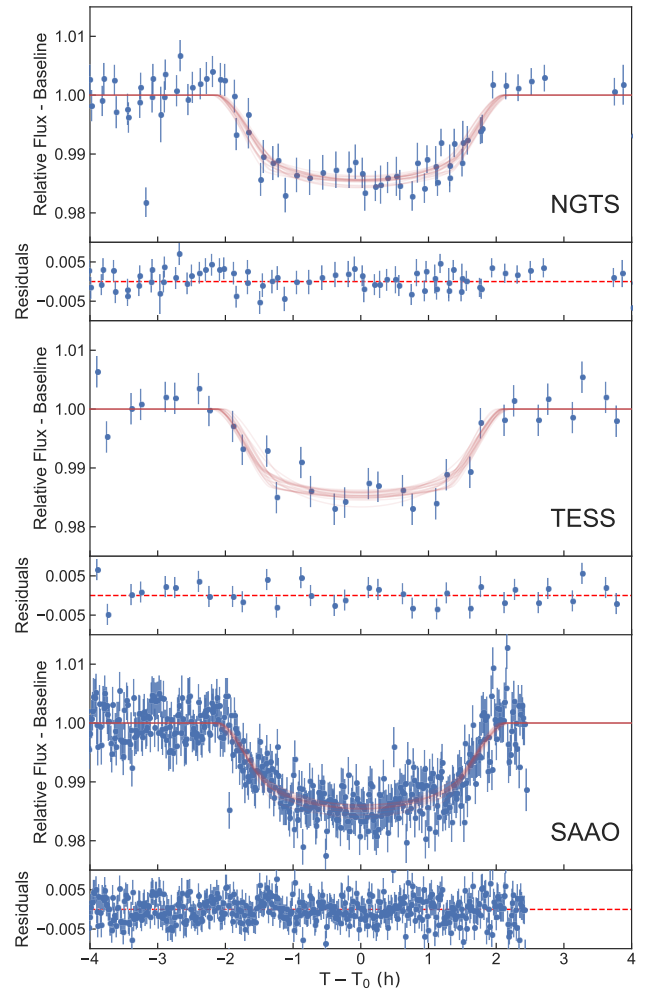


Figure 4. Data and model fits to the photometry from NGTS, TESS and SAAO-1m obtained using ALLESFITTER. The NGTS data is binned to 10 minutes, whereas the TESS and SAAO data are unbinned. The red line shows the model fit derived by ALLESFITTER, and the shaded region is the uncertainty in the model.

eters using the LDTK package (Parviainen & Aigrain 2015) for each photometric filter used, adopting limb darkening laws from Kipping (2013) in the fit.

We ran ALLESFITTER with 100 walkers going for 80000 steps. We found this to be more than sufficient for the MCMC to converge to a solution, ensuring that the chains were at least 30 times the autocorrelation length of each parameter. 10000 of these steps were discarded as burn in and not used when analysing the results. The modal values of the posterior distributions for each parameter were adopted as the most probable values, with the $1-\sigma$ (68.3 percent) confidence intervals taken as an estimate of uncertainty. The fitted parameters were then used to derive additional parameters for the system.

This global modelling reveals the companion in this system is a high mass brown dwarf, with a mass of $69.5^{+5.7}_{-5.4} M_{\text{Jup}}$ and radius of $1.034^{+0.055}_{-0.053} R_{\text{Jup}}$. The system is also notable for having a reasonably long period of $17.839654^{+0.000037}_{-0.000038}$ days, and a high level of eccentricity $0.3767^{+0.0061}_{-0.0061}$. We note that this period makes NGTS-19 the longest period transiting brown dwarf to be initially

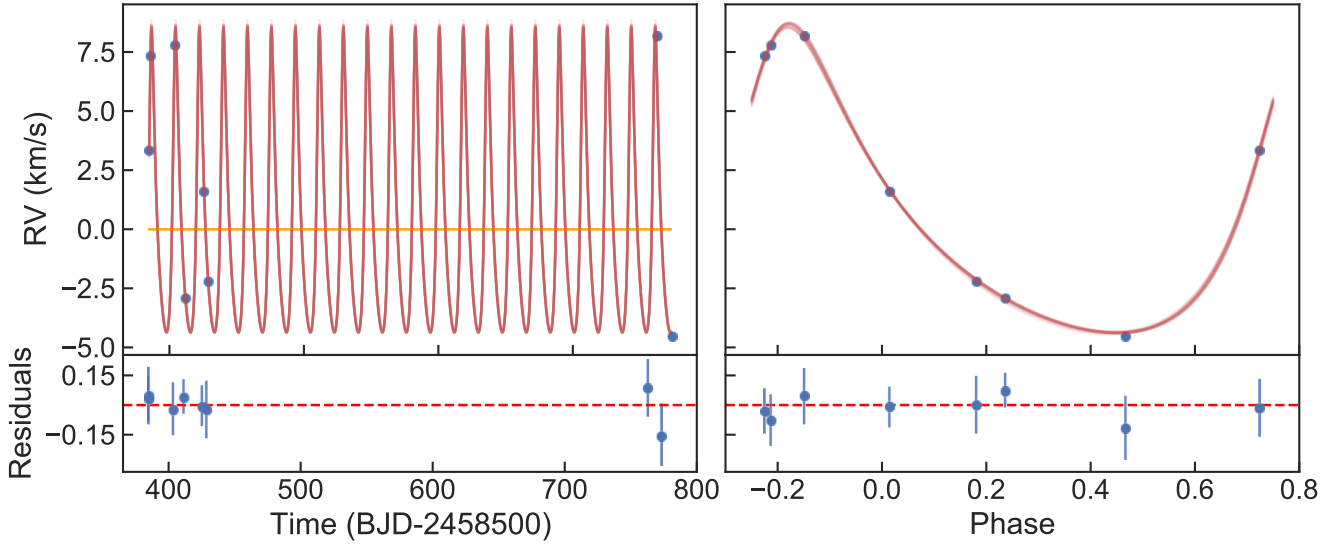


Figure 5. Data and model fits to the radial velocity measurements from CORALIE, obtained using ALLESFITTER. The CORALIE radial velocities have had the systemic velocity of the NGTS-19 system subtracted, and a jitter term has been added in quadrature to the error bars. The red line shows the model fit derived by ALLESFITTER, and the shaded region is the 1-sigma uncertainty in the model. The left panel shows the measurements in time series, and the right hand panel shows the radial velocities folded on the period determined by global modelling.

discovered using purely ground-based photometry, highlighting the value of the long observing baselines used by NGTS. The full list of fitted and derived parameters for the system is given in Table 5. The model fits to each set of data are shown in Figures 4 and 5.

4 DISCUSSION

4.1 Mass-Radius Relation

In Section 3.3 we determined that the companion to NGTS-19 is a high mass brown dwarf. This adds to the small, but growing number of objects being discovered in the so-called "brown dwarf desert". With direct measurements of the brown dwarf's mass and radius we can make a comparison with both the known population of transiting brown dwarfs, as well as with predictions from evolutionary models. In Figure 6, we compare the mass and radius of NGTS-19b to the known brown dwarf companions around main sequence stars from Carmichael et al. (2020a). We see that with a mass of $69.5^{+5.7}_{-5.4} M_{\text{Jup}}$, NGTS-19b lies at the upper end of the brown dwarf mass distribution, close to the substellar boundary.

When we compare the system to isochrones from Marley et al. (2018), we see that the system agrees well with the 0.4 Gyr model. This is in contrast to the age determination from the SED fit performed by ARIADNE, which predicted a much older system age of $8.5^{+3.2}_{-6.0}$ Gyr. This leaves us with two potential scenarios. It is possible that the system is indeed young, despite the age estimates from the SED. Alternatively, we may assume that the age from the SED fit is correct and the brown dwarf's radius has been inflated by some mechanism, making it appear younger in mass-radius space.

4.1.1 Possible youth of the system

An important parameter to know for any discovered transiting brown dwarf is the system age. To gain some estimate of this, we compare the mass and radius of NGTS-19b to evolutionary models from,

a variety of ages. We follow the method of Gillen et al. (2020), first interpolating between the models in order to compute a finer grid of model predictions and then comparing our global modelling results for the mass and radius of the system to this grid to compute an age estimate. For this, we use the Sonora brown dwarf models of Marley et al. (2018). Doing so yields an estimate for the age of the system of $0.46^{+0.26}_{-0.15}$ Gyr, this is not consistent with the determined age from ARIADNE, which predicts an older system.

Despite the small number of transiting brown dwarfs yet discovered, there are a reasonable number of young systems. These are often found in clusters, from which the age can be accurately determined (Gillen et al. 2017; Beatty et al. 2018; David et al. 2019). However there are known brown dwarfs orbiting young stars not associated with clusters, for example NGTS-7Ab (Jackman et al. 2019), with an age of just 55 Myr. Discoveries of brown dwarfs at these ages is important, as they will be undergoing gravitational contraction at a faster rate than at later ages (as seen by the large gaps between isochrones in Figure 6). This allows for some of the most powerful tests of brown dwarf evolutionary models.

This however does not explain the discrepancy seen between the age determined from the brown dwarf mass & radius, and that found in the SED fit. We note that the age determined from the SED by ARIADNE is poorly constrained, and is consistent with our inferred brown dwarf age at the 2σ level. To try and confirm or refute this age measurement, we checked for additional youth indicators. We examined the CORALIE spectrum for signs of Lithium absorption, which is typically an indicator of youth, however we find no such absorption in the spectrum. The star also has a relatively low $v \sin(i)$, which would also not suggest youth, and is not part of a known moving group. Thus the only evidence that the brown dwarf is young is its unusually large radius. This means that we cannot conclusively say that this is indeed a young system, as the radius of the brown dwarf could have been increased by some other means.

Table 5. Best fitting and derived parameters from the global modelling of NGTS-19 using ALLESFITTER. The values are derived from the modal values of the posterior distribution, with $1-\sigma$ uncertainties stated as errors. Note that the limb darkening coefficients are parameterised as in [Kipping \(2013\)](#)

Parameter	Symbol	Unit	Value
<i>Fitted Transit parameters</i>			
Scaled BD and Star Radii	$(R_* + R_{BD})/a$	—	$0.0359^{+0.0015}_{-0.0013}$
Radius ratio	R_{BD}/R_*	—	$0.1182^{+0.0037}_{-0.0035}$
Cosine inclination	$\cos i$	—	$0.0223^{+0.0018}_{-0.0019}$
Impact parameter	b	—	$0.730^{+0.033}_{-0.041}$
Epoch	T_0	HJD	$2458533.0207^{+0.0011}_{-0.0011}$
Period	P	days	$17.839654^{+0.000037}_{-0.000038}$
$\sqrt{e} \cos(\omega)$	f_c	—	$0.5322^{+0.0042}_{-0.0102}$
$\sqrt{e} \sin(\omega)$	f_s	—	$-0.306^{+0.014}_{-0.014}$
<i>Limb Darkening Parameters</i>			
NGTS LDC 1	$q_{1,NGTS}$		$0.64^{+0.22}_{-0.24}$
NGTS LDC 2	$q_{2,NGTS}$		$0.53^{+0.27}_{-0.29}$
TESS LDC 1	$q_{1,TESS}$		$0.37^{+0.25}_{-0.18}$
TESS LDC 2	$q_{2,TESS}$		$0.39^{+0.32}_{-0.25}$
SAAO LDC 1	$q_{1,SAAO}$		$0.37^{+0.29}_{-0.21}$
SAAO LDC 2	$q_{2,SAAO}$		$0.45^{+0.31}_{-0.28}$
<i>Radial Velocity Parameters</i>			
Systemic velocity	V_{sys}	km s^{-1}	$-33.9166^{+0.0097}_{-0.0105}$
RV semi-amplitude	K	km s^{-1}	$6.492^{+0.063}_{-0.062}$
<i>Derived brown dwarf parameters:</i>			
Brown dwarf mass	M_{BD}	M_{Jup}	$69.5^{+5.7}_{-5.4}$
Brown dwarf radius	R_{BD}	R_{Jup}	$1.034^{+0.055}_{-0.053}$
Brown dwarf density	ρ_{BD}	g cm^{-3}	77^{+17}_{-13}
Semi-major axis	a	AU	$0.1296^{+0.0074}_{-0.0072}$
Scaled Semi-major axis	a/R_*	—	$27.9^{+1.6}_{-1.6}$
Inclination	i	Degrees	$88.72^{+0.11}_{-0.11}$
Orbital Eccentricity	e	—	$0.3767^{+0.0061}_{-0.0061}$
Argument of Periastron	ω	Degrees	$330.1^{+1.4}_{-1.3}$
Equilibrium Temp.	$T_{eq,BD}$	K	543^{+17}_{-16}
Transit Duration	t_{trans}	hours	$4.252^{+0.077}_{-0.074}$

4.1.2 Inflated Brown Dwarf Radii

It should be noted however, that the models used in Figure 6 are for isolated brown dwarfs, whereas here we have a brown dwarf with a close stellar companion. Therefore, it is possible that the system is indeed the age determined from the SED and NGTS-19b is inflated relative to model predictions. There are brown dwarfs with unusually large radii, however these are usually associated with being strongly irradiated (e.g [Zhou et al. 2019](#); [Sivervd et al. 2012](#)), although this is not always the case (e.g [Csizmadia et al. 2015](#)).

[Bouchy et al. \(2011\)](#) showed that unlike in the case of hot Jupiters, where stellar irradiation can play a large effect in inflating the radii of the companion ([Sestovic et al. 2018](#)), the effect is much smaller for brown dwarfs, particularly at the higher mass end. It is also worth noting that the brown dwarf they were analysing (CoRoT-15b) has an equilibrium temperature almost twice that of NGTS-19b. Hence it is even less likely to have an effect on the radius of this system. In Figure 7 we plot the relationship between the radius and equilibrium temperature for known brown dwarfs. We see that although there is perhaps a slight upwards trend in radius with increasing temperature it is not noticeably significant. When

compared to brown dwarfs with similar equilibrium temperatures, we see that the radius of NGTS-19b is not an outlier, and is well within the observed scatter. If NGTS-19b is truly an inflated brown dwarf then there must be some other means to have increased its radius other than purely irradiation from its host star.

It is important to note however that the orbit of NGTS-19b is highly eccentric, and thus the distance between the brown dwarf and its host star varies significantly. Based on the measured eccentricity and semi-major axis, we determine a periastron distance of 0.0817 AU, which is not too dissimilar to that of a hot Jupiter. Therefore it is possible that the increased irradiation experienced by the brown dwarf at periastron could act to inflate its radius. This eccentric orbit could also act to inflate the brown dwarf due to tidal effects exerted on it by the host star, as has been demonstrated for gas giant exoplanets ([Millholland et al. 2020](#)). However given the long period of the system, and the high mass of the brown dwarf, we determine it to be unlikely that these effects would transfer enough heat into the brown dwarf to inflate it.

[Casewell et al. \(2020\)](#) consider the white-dwarf brown-dwarf binary NLTT5036, which also shows signs of inflation. They show that regardless of the level or irradiation experienced, low mass brown-dwarfs ($M < 35M_{\text{Jup}}$) are able to be inflated when heated by their host star. However, higher mass brown-dwarfs are much harder to inflate, with the majority of them showing no inflation. The temperature of the host star also plays an important role here; hotter stars will emit more ultraviolet radiation whereas cooler stars will emit more in the infrared. NGTS-19, a mid K-dwarf, has an effective temperature of 4890 K which would leave it at the cooler end of the distribution of transiting brown dwarf host stars ([Carmichael et al. 2020a](#)), with no significant amount of either UV or IR radiation.

Stellar activity may also affect the ability of a brown-dwarf to be inflated by its host star. CoRoT-15b ([Bouchy et al. 2011](#)) and CoRoT-33b ([Csizmadia et al. 2015](#)) both show signs of being inflated, and are noted to be orbiting active host stars. This may suggest that brown-dwarf inflation is caused by a similar mechanism to M-dwarfs ([Stelzer et al. 2013](#)). However these two brown dwarfs both have large radii uncertainties (27% and 48% for CoRoT-15b and 33b respectively) so it is difficult to categorically say whether or not these systems are actually inflated. We note that NGTS-19 does not show any signs of significant stellar activity. In almost 150 nights of NGTS data we do not detect any obvious flares, and the CORALIE spectra do not show any signs of magnetic activity, such as $H\alpha$ emission. However to accurately characterise the stars magnetic field would require further investigation.

Another important factor to consider is metallicity. For a fixed mass and age, the radii of brown dwarfs increase with increasing metallicity. [Burrows et al. \(2011\)](#) show that a change from +0.0 dex to +0.5 dex in the metallicity of the brown dwarf can result in an increase in radius of as much as 0.1 R_{Jup} . Our analysis in Sections 3.1 and 3.2 suggest a small, but significant host star metallicity of around 0.1 dex. This may explain some of the discrepancy between model and measurement we see for NGTS-19b, but is unlikely to increase the radius by enough given the disagreement between our measured and predicted ages. They also show that differences between clear and cloudy brown dwarf models can cause deviations in radius by about 0.05 R_{Jup} , but this too is likely not substantial enough to account for the discrepancy seen in our measurements.

4.2 Eccentricity and Tidal Circularisation

NGTS-19b has a relatively large orbital eccentricity of $0.3767^{+0.0061}_{-0.0061}$ (Section 3.3). This is not necessarily unusual for

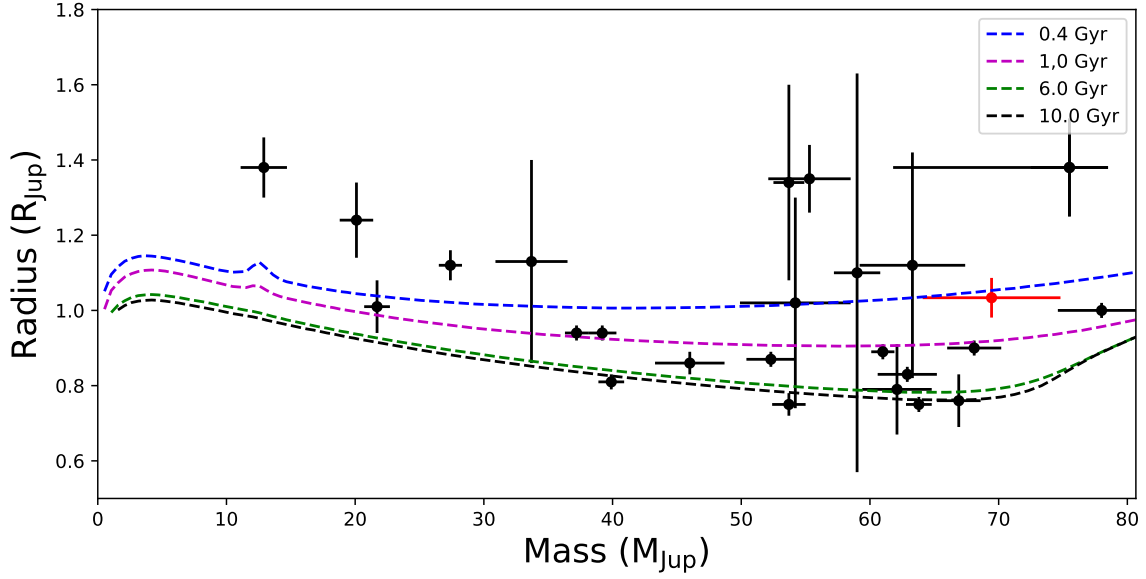


Figure 6. Mass-Radius relation for known brown dwarfs around Main Sequence stars from [Carmichael et al. \(2020a\)](#). NGTS-19b is plotted in red. Sonora model isochrones from [Marley et al. \(2018\)](#) for ages of 0.4, 1, 6 and 10 Gyr are plotted for comparison. Note that RIK 72b ([David et al. 2019](#)) is not shown due to its inflated radius of $3.1R_{\text{Jup}}$, nor is the brown dwarf binary system 2M0535-05a ([Stassun et al. 2006](#))

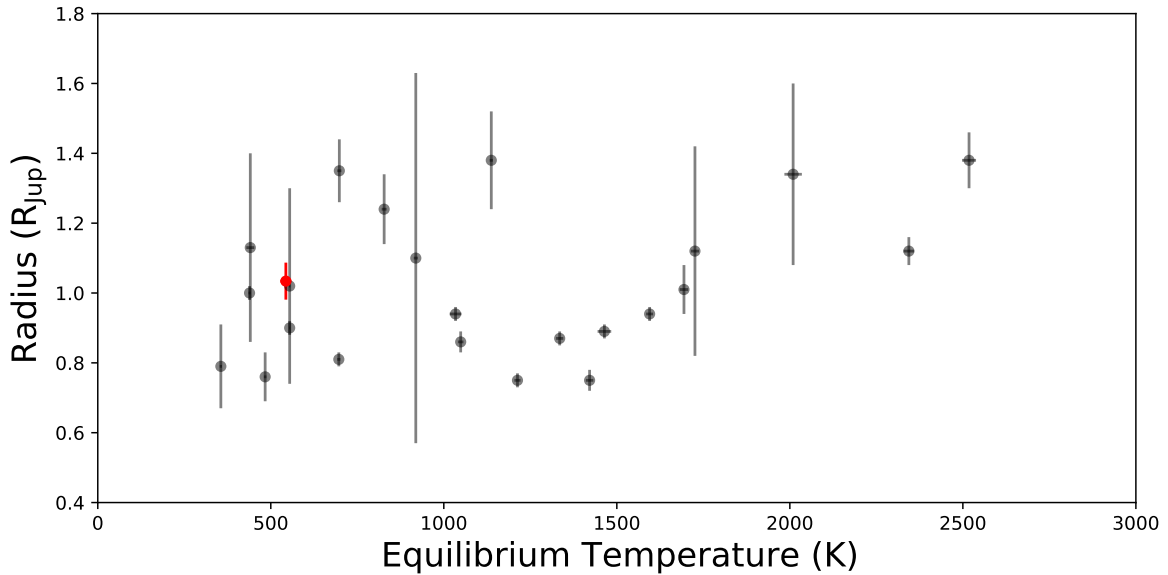


Figure 7. Relationship between equilibrium temperature and radius for known brown dwarfs around main sequence stars from [Carmichael et al. \(2020a\)](#). NGTS-19b is plotted in red. We use the effective temperature of the host star (if reported) and the relation in [Méndez & Rivera-Valentín \(2017\)](#) to calculate the time-averaged equilibrium temperature of the brown dwarf. For all systems we assume a Bond albedo of zero. Note that RIK 72b ([David et al. 2019](#)) is not shown due to its inflated radius of $3.1R_{\text{Jup}}$, nor is the brown dwarf binary system 2M0535-05a ([Stassun et al. 2006](#))

transiting brown dwarfs. Of the 27 transiting brown dwarfs listed by Carmichael et al. (2020a), 10 have eccentricity greater than 0.1. In Figure 8, we show the distribution of eccentricity as a function of orbital period for the population of transiting brown dwarfs. Only two known systems have a higher eccentricity than NGTS-19b, these are TOI-811b and KOI-415b (Carmichael et al. 2020a; Moutou et al. 2013) with orbital eccentricities of 0.4072 ± 0.046 and 0.689 ± 0.001 respectively. However with orbital periods of 25.2 and 166.8 days, these systems are both longer period than NGTS-19b and there is no known transiting brown dwarf with a shorter orbital period that has a higher degree of eccentricity.

For a system with a semi-major axis of just $0.1296^{+0.0074}_{-0.0072}$ AU, this is a reasonably high level of eccentricity. It is known that over the course of evolution of such small separation systems, the tidal effect of the host star acts to circularise the orbit. This was a process first applied to binary stars (Zahn & Bouchet 1989), but is equally applicable to brown dwarf and hot Jupiter systems (Rasio et al. 1996). We can apply this theory to NGTS-19b, to evaluate whether we would expect the orbit to have circularised, given the period and masses of the system. The majority of this orbital circularisation is expected to occur early in the lifetime of the system, therefore if we determine a short orbital circularisation timescale for NGTS-19b it could be an indicator that the system is indeed young as suggested in section 4.1.1.

We follow the method of Carmichael et al. (2020b), based on the theoretical framework of Jackson et al. (2008). Here the orbital circularisation timescales for the host star and brown dwarf are defined as

$$\frac{1}{\tau_{circ,*}} = \frac{171}{16} \sqrt{\frac{G}{M_*}} \frac{R_{BD}^5 M_{BD}}{Q_*} a^{-\frac{13}{2}}, \quad \text{and} \quad (1)$$

$$\frac{1}{\tau_{circ,BD}} = \frac{63}{4} \sqrt{\frac{GM_*^3 R_{BD}^5}{Q_{BD} M_{BD}}} a^{-\frac{13}{2}}, \quad (2)$$

where a is the semi-major axis of the system, and Q_* and Q_{BD} are the tidal quality factors for the star and brown dwarf respectively. From this, the circularisation timescale of the system is defined as

$$\frac{1}{\tau_e} = \frac{1}{\tau_{circ,*}} + \frac{1}{\tau_{circ,BD}}. \quad (3)$$

From this we can determine the circularisation timescale for the system. We note that this is typically applied to systems with lower eccentricities and shorter orbital periods than NGTS-19b. However, it is still a useful method for estimating whether or not we would expect a system of this type to have circularised in its lifetime. The tidal quality factors are rather poorly constrained in the literature, so as in Carmichael et al. (2020b) we adopt a lower bound on Q_{BD} of $10^{4.5}$ based on the work of Beatty et al. (2018) on CWW 89Ab. We place a lower bound of 10^5 on Q_* based on previous studies of binary stars (Meibom & Mathieu 2005; Milliman et al. 2014).

In Table 6 we show the circularisation timescale for various combinations of both stellar and brown dwarf tidal quality factors. We find that there is no combination of tidal quality factors that provide a circularisation timescale of less than 18 Gyr, given the lower bounds we have placed. In fact, almost all combinations give a large circularisation timescale. Unless the tidal quality factors are substantially smaller than our lowest estimates (by at least an order

Table 6. Tidal circularisation timescale for NGTS-19b based on the tidal circularisation model of Jackson et al. (2008), for a combination of reasonable stellar and brown dwarf tidal quality factors. For no realistic combination of tidal quality factors do we find a circularisation timescale that is reasonable.

Q_*	Q_{BD}	τ_e (Gyr)
10^5	$10^{4.5}$	18.39
10^6	$10^{4.5}$	169.10
10^7	$10^{4.5}$	934.54
10^5	10^5	18.52
10^6	10^5	180.18
10^5	10^6	18.58
10^6	10^6	185.23
10^7	10^6	1801.78

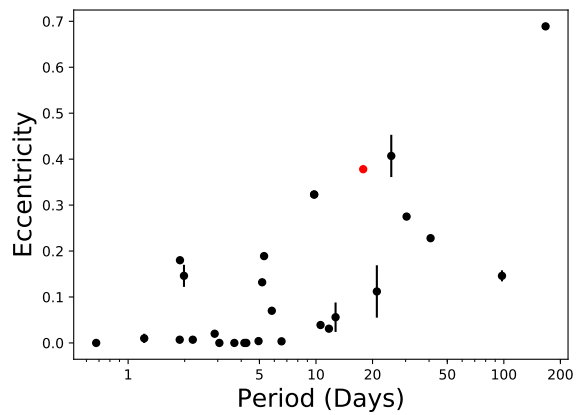


Figure 8. Eccentricity against period for known transiting brown dwarfs orbiting main sequence stars from Carmichael et al. (2020a). NGTS-19b is indicated in red.

of magnitude), we conclude that we would not expect the system to have been tidally circularised, and thus finding a brown dwarf of this orbital period and eccentricity is not unusual.

4.3 Future observing prospects

4.3.1 Secondary Eclipse of NGTS-19b

It would be particularly valuable to our understanding on NGTS-19b if we were able to detect a secondary eclipse of the brown dwarf. Doing so would allow for direct determination of the brown dwarf temperature (as shown in Jackman et al. (2019)). However, due to the significant difference in luminosity between the host star and the fainter brown dwarf, making such a detection is difficult.

For an eccentricity of $0.3767^{+0.0061}_{-0.0061}$ (assuming the argument of periastron in table 5), we would expect to see a secondary eclipse at around phase $0.7075^{+0.0055}_{-0.0055}$. Both NGTS and TESS observations have coverage at this phase, so we examined their lightcurves for evidence of this secondary eclipse (Figure 9). Despite the level of scatter in both lightcurves being very small ($<0.1\%$) for an object this faint, there is no obvious sign of a secondary eclipse seen in either of the lightcurves. Indeed we searched a large range of orbital phase to account for any error in our calculation of orbital eccentricity, and we see no evidence for a secondary eclipse at any point. We note that for some objects in eccentric orbits you do not see a secondary eclipse at all, due to the system configuration and

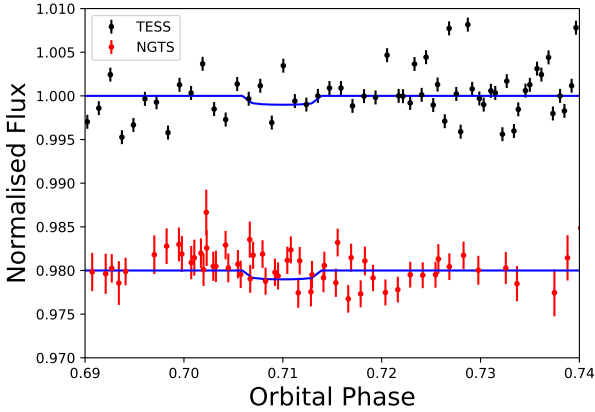


Figure 9. NGTS and TESS photometry for NGTS-19 around the expected phase of the secondary eclipse of the system. The NGTS data is binned to 30 minutes for comparison with the TESS full frame image data. Over plotted in blue is a model of the maximum depth secondary eclipse for comparison. No obvious secondary eclipse is seen in either of the lightcurves.

inclination. However this is not the case for NGTS-19b where we would expect to see a secondary if the object had a high enough surface brightness, based on our modelling.

Based on the atmospheric models of Baraffe et al. (2003), an isolated $0.07 M_{\odot}$ brown dwarf has an effective temperature of 1626 K at 10 Gyr. If the system is young as speculated in Section 4.1, then the temperature could instead be as high as 2335 K. This leads to predicted secondary eclipse depths of $\approx 0.008\%$ and $\approx 0.09\%$ respectively. This is within the scatter of both the NGTS and TESS lightcurves, and suggests that a non-detection is not unexpected. Due to the faint nature of this system, the detection of such a shallow secondary eclipse would be extremely challenging, even if the system is younger and more luminous than we expect. Based on this lack of secondary eclipse detection, we can place a tentative upper limit of ~ 2800 K on the brown dwarf temperature. For a temperature greater than this we would expect the secondary eclipse to be large enough that it would be visible in the lightcurves. This places a lower limit on the age from the Baraffe et al. (2003) models of 0.1 Gyr, so is not sufficient to constrain confirm or refute the suggested youth of the system, i.e even if the brown dwarf is as young as suggested by its radius, we still would not expect to detect a secondary eclipse.

4.3.2 Spin-orbit angle

Transiting brown dwarfs present an interesting avenue to help understand the distribution seen in spin orbit angle seen for exoplanets and low mass stars. By measuring the Rossiter-McLaughlin effect, it has been shown that hot Jupiters can show a wide range of spin-orbit angles, with some even showing retrograde orbits (Queloz et al. 2010). However, similar studies of this effect for low mass stars has shown that these systems do tend to be aligned (Triaud et al. 2013). This is likely due to the fact that hot Jupiters arrive into their short period orbits via dynamical interactions that force them into highly eccentric orbits that then circularise - leading to misalignment.

Brown dwarfs bridge the gap between planets and stars, so

measuring the spin orbit angle of transiting brown dwarfs allows for insight into what may cause the misalignment seen in planetary systems. For this system in particular, detection of a misaligned orbit may be some indication that the large eccentricity may not be primordial, and has been caused interactions with a third body via Lidov-Kozai cycles (Lidov 1962; Kozai 1962). This would provide valuable insight into how a system such as this has formed and evolved.

The semi-amplitude of the Rossiter-McLaughlin effect scales approximately with planet size and stellar rotational velocity, in the following relation (Triaud 2018)

$$A_{RM} \approx \frac{2}{3} D v \sin(i) \sqrt{1 - b^2} \quad (4)$$

Where D is the transit depth $(\frac{R_{BD}}{R_*})^2$, $v \sin(i)$ is the projected stellar rotation velocity, and b is the impact parameter. From analysis of the CORALIE spectra, we calculate $v \sin(i) = 2.1 \pm 0.4 \text{ km s}^{-1}$ for NGTS-19. This implies a Rossiter-McLaughlin amplitude of $13.4^{+2.7}_{-2.6} \text{ m s}^{-1}$. A signal of this magnitude could be detected easily with an instrument such as ESPRESSO (Pepe et al. 2021).

5 CONCLUSIONS

We report the discovery of a high mass brown dwarf companion on a $P = 17.839654^{+0.000037}_{-0.000038}$ day eccentric orbit around a main sequence K type star. NGTS-19b is a brown dwarf with a mass of $69.5^{+5.7}_{-5.4}$, placing it at the high end of the brown dwarf mass distribution. When compared to evolutionary models, the system is consistent with having an age of around 0.5 Gyr, although this is not consistent with age measurements from our spectroscopic or SED analysis, suggesting that the brown dwarf may be inflated due to interactions with its host star.

The system also has a highly eccentric orbit, with only 2 transiting brown dwarf systems being more eccentric. There are no shorter period, more eccentric transiting brown dwarfs known. When examined using established tidal circularisation theory, we find that the system has a long enough period that we would not expect it to have circularised in any reasonable time period.

NGTS-19b is the 29th transiting brown dwarf to be discovered, adding to the population of companions to main sequence stars known as the brown dwarf desert. With the continuing survey of the TESS mission it is quite possible that there will be many more additions to this once sparse region of parameter space in the years to come.

ACKNOWLEDGEMENTS

Based on data collected under the NGTS project at the ESO La Silla Paranal Observatory. The NGTS facility is operated by the consortium institutes with support from the UK Science and Technology Facilities Council (STFC) under projects ST/M001962/1 and ST/S002642/1.

This paper includes data collected by the TESS mission. Funding for the TESS mission is provided by the NASA Explorer Program.

This paper uses observations made at the South African Astronomical Observatory (SAAO).

JA is supported by an STFC studentship. This work has been

carried out within the framework of the National Centre of Competence in Research PlanetS supported by the Swiss National Science Foundation. JSJ acknowledges support by FONDECYT grant 1201371, and partial support from CONICYT project Basal AFB-170002. MNG acknowledges support from MIT's Kavli Institute as a Juan Carlos Torres Fellow. EG gratefully acknowledges support from the David and Claudia Harding Foundation in the form of a Winton Exoplanet Fellowship.

DATA AVAILABILITY

The data underlying this article will be shared on reasonable request to the corresponding author.

REFERENCES

- Allard F., Homeier D., Freytag B., 2012, *Philosophical Transactions of the Royal Society A: Mathematical, Physical and Engineering Sciences*, 370, 2765
- Baraffe I., Chabrier G., Allard F., Hauschildt P. H., 2002, *A&A*, 382, 563
- Baraffe I., Chabrier G., Barman T. S., Allard F., Hauschildt P. H., 2003, *A&A*, 402, 701
- Barbary K., 2016, *Journal of Open Source Software*, 58
- Bayliss D., et al., 2017, *AJ*, 153, 15
- Beatty T. G., Morley C. V., Curtis J. L., Burrows A., Davenport J. R. A., Montet B. T., 2018, *AJ*, 156, 168
- Blanco-Cuaresma S., Soubiran C., Heiter U., Jofré P., 2014, *A&A*, 569, A111
- Borucki W. J., et al., 2010, *Science*, 327, 977
- Bouchy F., et al., 2011, *A&A*, 525, A68
- Burrows A., Heng K., Nampaisarn T., 2011, *ApJ*, 736, 47
- Carmichael T. W., Latham D. W., Vanderburg A. M., 2019, *AJ*, 158, 38
- Carmichael T. W., et al., 2020a, arXiv e-prints, p. arXiv:2009.13515
- Carmichael T. W., et al., 2020b, *AJ*, 160, 53
- Casewell S. L., Debes J., Braker I. P., Cushing M. C., Mace G., Marley M. S., Kirkpatrick J. D., 2020, *MNRAS*, 499, 5318
- Castelli F., Kurucz R. L., 2004, preprint, (arXiv:0405087)
- Chaushev A., et al., 2019, *MNRAS*, 488, 5232
- Choi J., Dotter A., Conroy C., Cantiello M., Paxton B., Johnson B. D., 2016, *ApJ*, 823, 102
- Coppejans R., et al., 2013, *PASP*, 125, 976
- Csizmadia S., et al., 2015, *A&A*, 584, A13
- Cumming A., Butler R. P., Marcy G. W., Vogt S. S., Wright J. T., Fischer D. A., 2008, *PASP*, 120, 531
- David T. J., Hillenbrand L. A., Gillen E., Cody A. M., Howell S. B., Isaacson H. T., Livingston J. H., 2019, *ApJ*, 872, 161
- Folkes S. L., et al., 2012, *MNRAS*, 427, 3280
- Foreman-Mackey D., Hogg D. W., Lang D., Goodman J., 2013, *PASP*, 125, 306
- Gaia Collaboration et al., 2018, *A&A*, 616, A1
- Gill S., et al., 2020, *ApJ*, 898, L11
- Gillen E., Hillenbrand L. A., David T. J., Aigrain S., Rebull L., Stauffer J., Cody A. M., Queloz D., 2017, *ApJ*, 849, 11
- Gillen E., Hillenbrand L. A., Stauffer J., Aigrain S., Rebull L., Cody A. M., 2020, *MNRAS*, 495, 1531
- Grether D., Lineweaver C. H., 2006, *ApJ*, 640, 1051
- Günther M. N., Daylan T., 2019, Allesfitter: Flexible Star and Exoplanet Inference From Photometry and Radial Velocity, Astrophysics Source Code Library (ascl:1903.003)
- Günther M. N., Daylan T., 2020, arXiv e-prints, p. arXiv:2003.14371
- Hauschildt P. H., Allard F., Baron E., 1999, *ApJ*, 512, 377
- Husser T.-O., Wende-von Berg S., Dreizler S., Homeier D., Reiners A., Barman T., Hauschildt P. H., 2013, *A&A*, 553, A6
- Jackman J. A. G., et al., 2019, *MNRAS*, 489, 5146
- Jackson B., Greenberg R., Barnes R., 2008, *ApJ*, 678, 1396
- Jenkins J. S., et al., 2015, *MNRAS*, 453, 1439
- Kipping D. M., 2013, *MNRAS*, 435, 2152
- Kovács G., Zucker S., Mazeh T., 2016, BLS: Box-fitting Least Squares, Astrophysics Source Code Library (ascl:1607.008)
- Kozai Y., 1962, *AJ*, 67, 591
- Kurucz R. L., 1993, VizieR Online Data Catalog, 6039
- Lidov M. L., 1962, *Planet. Space Sci.*, 9, 719
- Marcy G. W., Butler R. P., 2000, *PASP*, 112, 137
- Marley M., Saumon D., Morley C., Fortney J., 2018, Sonora 2018: Cloud-free, solar composition, solar C/O substellar atmosphere models and spectra, doi:10.5281/zenodo.1309035, https://doi.org/10.5281/zenodo.1309035
- Marted P. F. L., 2016, *A&A*, 591, A111
- Meibom S., Mathieu R. D., 2005, *ApJ*, 620, 970
- Meisner A. M., et al., 2020, *ApJ*, 899, 123
- Méndez A., Rivera-Valentín E. G., 2017, *ApJ*, 837, L1
- Millholland S., Petigura E., Batygin K., 2020, *ApJ*, 897, 7
- Milliman K. E., Mathieu R. D., Geller A. M., Gosnell N. M., Meibom S., Platais I., 2014, *AJ*, 148, 38
- Moutou C., et al., 2013, *A&A*, 558, L6
- Nakajima T., Oppenheimer B. R., Kulkarni S. R., Golimowski D. A., Matthews K., Durrance S. T., 1995, *Nature*, 378, 463
- Nielsen E. L., et al., 2019, *AJ*, 158, 13
- Nowak G., et al., 2017, *AJ*, 153, 131
- Palle E., et al., 2021, arXiv e-prints, p. arXiv:2103.11150
- Parsons S. G., et al., 2018, *MNRAS*, 481, 1083
- Parviainen H., Aigrain S., 2015, *MNRAS*, 453, 3821
- Pearson S., Scholz A., Teixeira P. S., Mužić K., Eislöffel J., 2020, *MNRAS*, 499, 2292
- Pecaut M. J., Mamajek E. E., 2013, *ApJS*, 208, 9
- Pepe F., et al., 2021, *A&A*, 645, A96
- Phillips M. W., et al., 2020, *A&A*, 637, A38
- Pinfield D. J., et al., 2008, *MNRAS*, 390, 304
- Queloz D., et al., 2000, *A&A*, 354, 99
- Queloz D., et al., 2010, *A&A*, 517, L1
- Rasio F. A., Tout C. A., Lubow S. H., Livio M., 1996, *ApJ*, 470, 1187
- Rebolo R., Zapatero Osorio M. R., Martín E. L., 1995, *Nature*, 377, 129
- Reylé C., 2018, *A&A*, 619, L8
- Ricker G. R., et al., 2015, *Journal of Astronomical Telescopes, Instruments, and Systems*, 1, 014003
- Rickman E. L., et al., 2019, *A&A*, 625, A71
- Saumon D., Marley M. S., 2008, *ApJ*, 689, 1327
- Schlafly E. F., Finkbeiner D. P., 2011, *Astrophysical Journal*, 737
- Schlegel D. J., Finkbeiner D. P., Davis M., 1998, *ApJ*, 500, 525
- Schneider A. C., et al., 2020, *ApJ*, 898, 77
- Sestovic M., Demory B.-O., Queloz D., 2018, *A&A*, 616, A76
- Sivert R. J., et al., 2012, *ApJ*, 761, 123
- Skrutskie M. F., et al., 2006, *AJ*, 131, 1163
- Spiegel D. S., Burrows A., Milsom J. A., 2011, *ApJ*, 727, 57
- Stassun K. G., Mathieu R. D., Valenti J. A., 2006, *Nature*, 440, 311
- Stassun K. G., et al., 2019, *AJ*, 158, 138
- Stelzer B., Marino A., Micela G., López-Santiago J., Liefke C., 2013, *MNRAS*, 431, 2063
- Tamuz O., Mazeh T., Zucker S., 2005, *MNRAS*, 356, 1466
- TriAUD A. H. M. J., 2018, The Rossiter-McLaughlin Effect in Exoplanet Research. p. 2, doi:10.1007/978-3-319-55333-7_2
- TriAUD A. H. M. J., et al., 2013, *A&A*, 549, A18
- TriAUD A. H. M. J., et al., 2017, *A&A*, 608, A129
- Vigan A., et al., 2020, arXiv e-prints, p. arXiv:2007.06573
- Vines J. I., Jenkins J. S., 2021, in prep
- Wheatley P. J., et al., 2018, *MNRAS*, 475, 4476
- Wright E. L., et al., 2010, *AJ*, 140, 1868
- Yee S. W., Petigura E. A., von Braun K., 2017, *ApJ*, 836, 77
- Zahn J. P., Bouchet L., 1989, *A&A*, 223, 112
- Zhou G., et al., 2019, *AJ*, 157, 31

This paper has been typeset from a $\text{\TeX}/\text{\LaTeX}$ file prepared by the author.